SPE 139524

Experimental and Numerical Simulation of CO_2 Injection Into Upper-Triassic Sandstones in Svalbard, Norway

R. Farokhpoor, O.Torsæter, T.Baghbanbashi, NTNU, A. Mørk, SINTEF, NTNU, E. Lindeberg, SINTEF

This paper was prepared for presentation at the SPE International Conference on CO_2 Capture, Storage, and Utilization held in New Orleans, Louisiana, USA, 10–12 November 2010.

Abstract

Sequestration of carbon dioxide in a saline aquifer is currently being evaluated as a possible way to handle carbon dioxide emitted from a coal-fuelled power plant in Svalbard. The chosen reservoir is a 300 m thick, laterally extensive, shallow marine formation of late Triassic-mid Jurassic age, located below Longyearbyen in Svalbard. The reservoir consists of 300 m of alternating sandstone and shale and is capped by 400 meter shale.

Experimental and numerical studies have been performed to evaluate CO_2 storage capacity and long term behaviour of the injected CO_2 in rock pore space. Laboratory core flooding experiments were conducted during which air was injected into brine saturated cores at standard conditions. Analysis of the results shows that the permeability is generally less than 2 millidarcies and the capillary entry pressure is high. For most samples, no gas flow was detected in the presence of brine, when employing a reasonable pressure gradient. This poses a serious challenge with respect to achieving viable levels of injectivity and injection pressure.

A conceptual numerical simulation of CO_2 injection into a segment of the planned reservoir was performed using commercial reservoir simulation software and available petrophysical data. The results show that injection using vertical wells yields the same injectivity but more increases in field pressure compare to injection through horizontal wells. In order to keep induced pressure below top-seal fracturation pressure and preventing the fast propagation and migration of CO_2 plume, slow injection through several horizontal wells into the lower part of the “high” permeability beds appears to offer the best solution.

The high capillary pressure causes slow migration of the CO_2 plume, and regional groundwater flow provides fresh brine for CO_2 dissolution. In our simulations, half of the CO_2 was dissolved in brine and the other half dispersed within a radius of 1000 meter from the wells after 4000 years. Dissolution of CO_2 in brine and lateral convective mixing from CO_2 saturated brine to surrounding fresh brine are the dominant mechanisms for CO_2 storage in this specific site and this guarantees that the CO_2 plume will be stationary for thousands of years.

Introduction

One of the strategies to mitigate climate change is to reduce atmospheric greenhouse gases by capturing and sequestering CO_2 in sub-surface reservoirs for extended periods of time. Saline aquifers are considered to be one of the best options for CO_2 sequestration due to their large storage capacity, injectivity potential and proximity to CO_2 sources at some places. Uncertainties due to limitation of geological data and reservoir data will, however, limit the accuracy of predictions from

modeling. (Bachu, et al., 2009). CO_2 sequestration in saline aquifers is being actively pursued particularly in United States, Norway, Germany, Canada, Algeria, Australia and Japan (Australian Cooperative Research Centres).

During the injection phase, the movement of CO_2 is governed by viscous forces and thereby by relative permeability. Once injection ceases, buoyancy driven migration is dominant. As the CO_2 rises, it leaves behind a residual phase trapped by capillary forces. When CO_2 encounters a low permeability layer or top seal, it spreads out and moves laterally in regionally extensive brine formation (Oloruntobi, et al., 2009). Most obviously, as the gas phase migrates upwards, it mixes with a larger volume of brine, and therefore more of it dissolves. Hydraulic dispersion and convective mixing effect may allow more carbon dioxide from the gas phase to dissolve in the aqueous phase (Lindeberg, et al., 1997). Carbon dioxide when dissolved in water forms a weak acid, which can react with the host rock and either dissolve or precipitate minerals (Ennis-King, et al., 2002).

Svalbard is located on the north-western margin of the Barents Shelf. Its main settlement, Longyearbyen, could be the first community in the world with no net CO_2 emissions (Sand and Braathen, 2006). The coal-fired power plant in Longyearbyen is small, annual CO_2 emission averaging 85000 tons/year, making it well-suited for test purposes. Svalbard has strict environmental laws, and with worldwide attention focused on the rapid impact of climate change in the arctic, handling CO_2 here provides a show-case for environmental policies, technologies and industries (Braathen, et al., 2009) These considerations formed the background for establishing the Longyearbyen CO_2 laboratory – a joint effort by academic institutions and industy to establish a test facility for CO_2 capture and injection in Longyearbyen.

The purpose of this paper is to perform a conceptual study of reservoir behaviour and optimal injection strategy of the intended sequestration target when using a scenario only based on the overall reservoir geometry and measured rock petrophysics. It should be emphasized that some factors such as segmentation of the reservoir and fractures, both known to significantly influence behaviour of the reservoir are not included here.

Geological setting

The intended storage site is located in the Upper Triassic – Middle Jurassic Kapp Toscana Group. The Kapp Toscana Group is capped by 400 m shale, forming substantial top seal for the reservoir. As part of Longyearbyen CO_2 Lab, four wells, labeled Dh1 to Dh4, have been drilled and fully cored in the vicinity of Longyearbyen; Dh1 and Dh3 were terminated above the reservoir, whereas Dh2 penetrated only as far as the upper part of the reservoir. The final well Dh4 was terminated close to the base of the De Geerdalen Fm., retrieving 298 m core section from the Kapp Toscana Group.

In well Dh4, the Kapp Toscana Group, encountered between 672 and 970 m depth, consists of the Knorringfjellet and the underlying De Geerdalen formations. The Knorringfjellet Fm. represents a condensed sedimentary succession with numerous hiati; reflecting a succession of regressive and transgressive events over a prolonged period of time. Its thickness is fairly uniform; ranging from 22 m in outcrops 44 km west of Longyearbyen to 21.5 m Dh2, 23.7 m in Dh4, 8 km to the east, to 15 m in outcrops 15 km northeast of Longyearbyen. The underlying De Geerdalen Formation consists of shallow marine, deltaic and lagoonal deposits. Both in core section and in outcrops (Mørk, et al., 1982; 1999), the De Geerdalen Formation exhibits units of fine to very fine sandstone of varying thickness alternating with mudstones. In Dh4 this unit is encountered in the lowermost 274 m of the well.

Within the Knorringfjellet and De Geerdalen formations, there are four potential intervals for CO_2 injection: The entire Knorringfjellet Formation and three predominantly sandy intervals in the De Geerdalen Formation. Samples from these four intervals (labeled interval 1 to 4 from top to bottom) reflect a spread in grain size, shale content and reservoir properties, as described in detail in the next section. The general facies log of potential intervals of the Kapp Toscana Group as logged in Dh4 is described though a series of facies, as shown in **Figure 1**.

Sample analysis

A total of 51 samples of core material from well Dh4 were collected and tested to determine reservoir properties. The bulk of these samples are from the uppermost three of the four intervals identified as likely to be suitable for injection.

The porosity of the cleaned and dried core plug samples was calculated using helium porosimetry and brine saturation (see below); permeability was measured using air flow. The resulting porosity and permeability data for all 51 samples are listed in **Table 1** and plotted in **Figure 2**. Porosity values range from 5 to 20 percent, whereas measured permeability ranged from not measurable to 2 mD. In general, the most permeable samples were found in interval 1. Most of the samples from interval 2 did not show air flow when using a 20 bar pressure gradient. Permeability of these samples is likely to be on the order of microdarcies. The samples from interval 4 show the lowest porosity and permeability. Sample porosity was also measured using brine saturation. Measured brine porosities were in general lower than the helium porosities especially for samples from interval 1. It was also observed that samples consisting of poorly sorted, weakly consolidated sands where prone to disintegrate after having been saturated with brine.

Samples were plugged in both vertical and horizontal orientation. Permeability measurements are performed in the direction of the core drilling. It is important to know the permeability variation with core direction. For this reason, horizontal oriented core is drilled from a vertically plugged core with biggest diameter. The permeability test shows double flow rate in horizontal direction compared to the flow in the vertical direction for that specific core plug.

The centrifuge method was used to measure the capillary pressure of water saturated samples. Normally, samples are centrifuged at a certain rate of speed until no more water is produced. This may commonly take 4-6 hours. For these very tight sandstones this procedure took up to 24 hours to complete, and the complete measurements for each core plug took two weeks. Capillary pressure tests were performed on six samples from intervals 1 and 2 (see **Table 2** for capillary pressure data for two samples). The long core samples were divided in two core plugs and placed in the centrifuge core holder. **Figure 3** shows the drainage capillary pressure versus average water saturation for samples from the first and second intervals. The differences observed in the capillary pressure curves are due to different pore size distribution. The core with the highest permeability in the first interval shows lower capillary pressure at the same average water saturation. The minimum capillary entry pressure for the samples from interval 1 and 2 is around 1 and 5 bar respectively. As it is shown in Figure 3, the irreducible water saturation for the samples from the first interval is 40 percent and 50 percent for the second interval.

The procedure for performing an unsteady state drainage relative permeability test is:

1. Fully saturating the core with brine (brine density is 1.04 g/cm^3)
2. Desaturating by injecting dried air until no more water is produced
3. Recording water production and air injection rate at each time step

This procedure was performed on four samples from interval 1 and 2. For interval 2 samples, no air flow was observed in the presence of water at laboratory conditions when utilizing a 20 bar pressure gradient. This conforms to what was expected, as air-flow through dry cores from this interval was very small to negligible. For the samples from interval 1, which are the most porous and permeable samples, air injection just produced a small amount of water. Further air injection did not result in more water production. It appears that these samples quickly reach the level of irreducible water saturation. However, 80 percent of the water was still remaining in the core by comparing the volume of produced water and water bulk volume, while the irreducible water saturation which is measured by centrifuge for the same core was 40 percent of the pore volume. The weight of this partially extracted sample shows water saturation somewhat in between. It seems that the air cannot push water from the small pores and water evaporation is occurring.

For this reason, another approach was applied to 100% brine saturated cores:

1. Spinning the core at a certain speed in the centrifuge and recording appropriate water saturation
2. Passing air through the core at that water saturation at constant pressure gradient (20 bar)
3. Calculating air effective and relative permeability

This approach just gives relative permeability data for gas phase (see **Table 3**). **Figure 4** shows the drainage gas relative permeability curve for two cores from interval 1with different air permeabilities. The relative permeability curve consists of two elements:

1. The end point saturation: These samples show that 50 to 60 percent of original water in place can be replaced by injecting air.
2. The end point relative permeability: air end point relative permeability for the most permeable core is 0.62 while the moderately permeable core 0.24.

The significant difference in drainage relative permeability for the two cores from the same formation with apparently similar lithology and porosity shows that small scale heterogeneities control the behavior of displacement front.

Numerical simulation study

The numerical simulations of the CO_2 storage of a segment of the Upper Triassic sandstones use a conceptual, generic and simple 3D aquifer model. The intention of these simulation exercises was to study reservoir performance using a simplified set of geological boundary conditions. Thus the present scenario does not include the observed stratigraphic dip of 2-3 degrees to the SW, segmentation and extensive fracturing as identified in the actual reservoir. The petrophysical data input is limited to values derived from the samples analyzed in the present study.

The simulation tool employed in this study is ECLIPSE 2009. The simulator can accurately compute the physical properties (density, viscosity, compressibility, etc.) of pure and impure CO_2 as a function of temperature and pressure (Hurter, et al., 2007). With the CO2STORE option, three phases are considered: a CO_2 rich phase, an H_2O rich phase and a solid phase. The CO_2 rich phase is labeled the gas phase while the H_2O rich phase is labeled the liquid phase. Precise mutual solubilities of CO_2 in water (xCO_2) and water in the CO_2-rich phases (yH_2O) are calculated to match experimental data for CO_2-H_2O systems under typical CO_2 storage conditions: 12-100 ^oC and up to 600 bar (ECLIPSE, 2009). Water and gas phase diffusion coefficients for each component are used to specify molecular diffusion and cross-phase diffusion.

The salt components of the water or solid phase are tracked as part of the fluid system. With the SOLID option the components NaCl and $CaCl_2$ can be present in both the aqueous phase and the solid phase. Salt precipitation around the wellbore will have an impact on permeability and mobility of fluid phase, as an increase in solid saturation will hinder fluid flow. To model the decrease in mobility as a function of solid saturation, the mobility multiplier is used. This option represents two columns of solid saturation and corresponding mobility multiplier.

Model geometry and material properties. Two different numerical models were built to test two different injection strategies. **Model 1** is a closed reservoir with 20 km long, 10 km wide and 300 m thick, capturing a complete vertical segment of the De Geerdalen and Knorringfjellet formations (see **Figure 5**). The model utilizes a simplified stratigraphic model consisting of the four intervals identified as suitable for CO_2 injection (Figure 1), each with a single active cell layer, separated by three inactive layers. The well configuration consists of a single vertical well injecting CO_2 into the four perforated active layers. The number of fundamental grid blocks is 100×500×7. The grid block size near injection well is refined to 20 m long, 20 m wide with the interval thickness to improve accuracy on CO_2 injection behavior. Closed conditions are assigned to the all boundaries.

Model 2 which comes from the first layer of Model 1 represents only Knorringfjellet Formation (interval 1) with 24 m thickness and consists of eight layers with different porosity and permeability (see Figure 5). A horizontal well with 200 m length is placed at the centre of the model in the seventh layer. For this model, except the number of layers, everything is the same as Model 1. The top is horizontal level at 672 m depth. Initial reservoir temperature and pressure are 32 ^oC and 70 bar respectively at the top of the formation. An injection of CO_2 at a rate of 35000 Sm^3/day for 40 years was controlled by a maximum bottom-hole pressure (BHP) of 200 bars in order to avoid fracturing. Fluid components are CO_2, H_2O, NaCl and $CaCl_2$. Brine salinity and density are 250 g/l and 1164 kg/m^3 respectively. Reservoir rock porosity and permeability are derived from Table 1. Horizontal permeability is assumed to be three times higher than in vertical which is close to measured

ratio (2 times higher in horizontal direction) for a specific core plug. Capillary pressure and relative permeability data from **Table 2** and **3** were employed.

Simulation results. In Model 1 bottom hole pressure reaches to 200 bar in an early phase, forcing reduced injection rates due to the predefined bottom hole pressure limit, and then levels out at 28000 Sm^3/day for the rest of injection period. In Model 2 injection rate remains constant for 3 years before BHP tips 200 bar, which forces injection rate down, leveling off at 25000 Sm^3/day. After 40 years of injection, the total amount of injected CO_2 in Model 2 is $4.0 \cdot 10^8$ Sm^3 compared to $4.14 \cdot 10^8$ Sm^3 in Model 1 (see **Figure 6)**. The maximum field pressure increase in Model 1 is 90 bar compared to 72 bar in Model 2. At the end of injection, the reservoir pressure at the top of the formation above the injection point for the Model 1 and 2 reaches to 180 bar and 163 bar respectively (see **Figure 7**). Peak pressure (the maximum pressure at the top of the formation above the injection point) is well within safety limits to avoid fracturing of the caprock. In Model 1, right after the injection started, the CO_2 at each interval hits the top seal layer and then spreads out laterally while in Model 2, after 30 years, the CO_2 plume will reach to the top of the formation.

The simulation results illustrate that within the given set of simplified geological boundary conditions used in this scenario, utilizing both vertical well and horizontal well will give the same injectivity but different field pressure increase. Using a horizontal well positioned in the most permeable interval (Model 2) yields less pressure build up. To avoid that the induced pressure increase reaches seal-fracturation pressure and to prevent the fast propagation of CO_2 plume, the best strategy is to inject slowly at reasonable rate at the lowest part of interval 1 (Knorringfjellet Formation) using horizontal wells. With this strategy, after 40 years of CO_2 injection, around $4.0 \cdot 10^8$ Sm^3 of CO_2 can be injected which is equal to17500 ton per year on average. The maximum field pressure is 72 bar, just 2 bar higher than initial pressure. At the end of the injection period, 15 percent of the injected CO_2 is dissolved in the formation brine (**Figure 8**). The lateral extension of the gas plume enlarges the contact area with the aquifer brine and improves solubility (Ülker, et al., 2007). After 4000 years, half of the CO_2 is dissolved in brine and the other half has spread out within a radius of 1 km and 500 m around the well for Model 1 and Model 2 respectively (see **Figure 9**). The amount of CO_2 dissolution in the brine is overestimated due to numerical dispersion.

In theory, in the close neighborhood of the well, the CO_2 will evaporate the brine causing salt precipitation inside the pore spaces (Burton, et al., 2008). To investigate this phenomenon further, local grid refinement was introduced 10 meter around the well in both models. The minimum grid cell size in this local grid refinement segment is 5 cm long, 10 cm wide and the same layer thickness. At the end of CO_2 injection no significant salt precipitation is observed in Model 2. In Model 1, the maximum solid saturation in an area of 10 m around the wellbore is less than 30 percent of the pore space at the end of injection. This is because the CO_2 injection rate (35000 Sm^3/day) is insufficient to give significant salt precipitation. (Hurter, et al., 2007).

Wherever CO_2 has migrated, fluid composition in the aqueous phase has been changed by CO_2 dissolution in brine. The variations in fluid composition are significant around the well bore. **Table 4** shows the compositional change that has occurred within a radius of 1m around the wellbore in both models by the end of injection. The compositional alteration of pore fluids continues even after injection has stopped. The free CO_2 phase moves upwards due to buoyancy and mixes and dissolves into pristine brine and changing its composition. On the other hand, the salt composition at the place where CO_2 has been injected reverts back to its initial composition within 1000-2000 years. This behavior can be explained by vertical convective mixing effect. When CO_2 is dissolved in water, carbonic acid is produced and brine pH decreases (Hurter, et al., 2007). Initial pH of formation brine is 6.9. At 1000 m around the wellbore, the pH value of formation brine is approximately 3 after 4000 years.

Further discussion

A short injection tests in the Kapp Toscana Group showed that the rock has fairly good injectivity suggesting the presence of fractures. Based on injection test result, calculated effective permeability of the lowermost 100 m of the well (the worst part of it in terms of reservoir properties) yields an average effective permeability of minimum 150 mD. The plug samples are

taken outside the fractures in order to avoid breakage. There are fractures galore in the core and fractures all over the outcrop lining up with a regional stress pattern. The fractures in the core even show mm sized apertures and there are few evidences of cementation. Relevant points for further discussion include the orientation of the fractures and which fracture population(s) dominates the flow pattern. Another highly important issue is the interaction between fractures and the rock matrix.

Conclusion

1. Four potential sandstone intervals suitable for injecting CO_2 can be identified in the 298 m long cored section of Dh4.
2. Experimental measurements reveal that these sandstones are very tight. Porosity ranging from 5 to 20 percent; permeability from 0 to 2 mD.
3. The Uppermost 24 meters of the reservoir exhibit the highest porosity and permeability values.
4. Preliminary numerical simulation of a conceptual case utilizing only the experimentally derived petrophysical properties show that injecting CO_2 in an extensive reservoir with very low permeability is possible. The best strategy is to inject slowly in the bottommost layers of the interval with highest permeability using horizontal wells.
5. The high capillary forces prevent the mobilization of blobs of non-wetting phase. As the amount of trapped CO_2 increases, it mixes with a larger volume of brine, promoting further dissolution of CO_2. Regional groundwater flow provides new fresh brine for CO_2 dissolution. In our simulation, half of the CO_2 is dissolved in brine and the other half has spread out within a radius of 1000 meter around the well after 4000 years.
6. The numerical simulation has shown that CO_2 induced dry-out does not develop sufficiently. The main cause for this is that the amount of injected CO_2 is not large enough. Salt precipitation is negligible and has no significant effect on mobility.

Acknowledgments

This publication is number 1 from “The Longyearbyen CO_2-Lab”. The authors gratefully acknowledge the support from the BIGCO_2 project and we also would thank Jan Tveranger (UNI-CIPR) for his review of this work.

Reference

Australian Cooperative Research Centres CRC. [Online]. - www.CO2CRC.com.au\Demonstraiting CCS.

Bachu S. and Pooladi-Darvish M. Geological Storage of CO_2. - FEKETE, 2009.

Braathen, A.; Sand, G.; Mørk, A.; Bælum, K.; Jochmann, M.; Christiansen, H. CO_2 Storage in Svalbard- reservoir characteristics with implications for modeling CO_2 behavior [Report] // Longyearbyen, Svalbard , 2009.

Burton, M.; Kumar, N. and Bryant, S. Time-Dependent Injectivity During CO_2 Storage in Aquifers [Conference] // SPE 113937. - Oklahoma : Society of Petroleum Engineers, 2008.

ECLIPSE Technical Description. - 2009.

Ennis-King, J. and Paterson, L. Engineering Aspects of Geological Sequestration of Carbon Dioxide [Conference] // SPE 77809. - Melbourne : Society of Petroleum Engineers, 2002.

Hurter, S.; Labregere, D. and Berge J. Simulations for CO_2 Injection Projects With Compositional Simulator [Conference] // SPE 108540. - Aberdeen : Society of Petroleum Engineering, 2007.

Lindeberg, E. and Wessel-Berg, D. Vertical Convection in an Aquifer Column Under a Gas Cap of CO_2 [Journal] // Eneregy Convers Mgmt. 38, S229-S234, 1997.

Mørk, A.; Dallmann, W.K.; Dypvik, H.; Johannessen, E.P.; Larssen, G.B.; Nagy, J.; Nøttvedt, A.; Olaussen, S.; Pchelina, T.M.; Worsley, D. Mesozoic lithostratigraphy. In: Dallmann, W.K. (ed.), Lithostratigraphic lexicon of Svalbard. Review and recommendations for nomenclature use. Upper Palaeozoic to Quaternary bedrock [Book] // Norsk Polarinstitutt, 1999. - Vols. 127-214.

Mørk, A.; Knarud, R. and Worsley, D. Depositional and diagenetic enviroments of the Triassic and lower Jurassic succession of Svalbard [Book] // Canadian Society of Petroleum Geologist, 1982.

Oloruntobi, O.S. and LaForce, T. Effect of Aquifer Heterogeneity on CO_2 Sequestration [Conference] // SPE 121776. - Amsterdam :

Society of Petroleum Engineering, 2009.

Sand, G. and Braathen, A. CO_2-fritt Svalbard i 2025 [Report] // Svalbardposten, 2006.

Tveranger, J.; Mørk, A. and Nemec, W. Sedimentary facies of DH4, Longyearbyen CO_2 project [Report] // CIPR, 2009.

Ülker, B.; Alkan, H. and Pusch, G. Implications of the Phase-Solubility Behaviour on the Performance Predictions of the CO_2 Trapping in Depleted Gas Reservoirs and Aquifers [Conference] // SPE 107189. - London : Society of Petorleum Engineering, 2007.

Table 1: porosity and permeability data

Depth (m)	*Porosity (%)*	*Permeability (md)*	*Depth (m)*	*Porosity (%)*	*Permeability (md)*
672.50	7.35	0.03	**771.14**	13.18	No Flow
673.68	5.73	0.09	**776.22**	13.04	0.045
674.38	14.73	0.14	**779.07**	10.18	0.02
674.95	18.68	1.79	**780.40**	13.82	0.032
675.49	18.06	1.11	**780.60**	10.5	0.022
676.30	16.47	1.17	**783.00**	4.79	No Flow
676.88	16.64	1.78	**784.30**	8.99	No Flow
677.14	15.92	0.61	**788.22**	12.39	No Flow
677.92	15	0.097	**791.10**	10.11	No Flow
678.32	10.54	0.57	**791.86**	8.43	No Flow
678.88	13.12	0.047	**792.09**	13.16	No Flow
680.27	8.73	0.09	**799.16**	10.43	No Flow
681.59	12.47	0.1	**803.29**	8.79	No Flow
682.08	13.9	0.82	**857.50**	16.1	0.051
682.27	12.53	0.22	**858.31**	14.72	0.071
687.22	8.95	0.056	**858.38**	11.21	0.04
688.45	18.71	0.025	**859.34**	14.64	0.095
688.71	8.97	No Flow	**860.44**	13.57	0.051
691.72	9	0.68	**867.76**	8.17	No flow
692.38	11.05	No Flow	**875.36**	15.67	0.126
694.08	19.62	0.73	**875.93**	10.83	0.07
695.11	11.21	0.04	**897.08**	8.37	No flow
695.25	14.67	0.06	**900.97**	10.41	No flow
695.28	16.53	0.25	**920.70**	2.31	No flow
705.25	13.05	No Flow	**969.64**	5.93	No flow
762.20	6.2	No Flow			

Table 2: Drainage capillary pressure data for air-water system for two samples from different depths

Sample from depth = 677		*Sample from depth = 780*	
Water Saturation	**Capillary Pressure (bar)**	**Water Saturation**	**Capillary Pressure (bar)**
1.00	0.00	1.00	0.00
0.96	0.17	0.97	0.17
0.96	0.67	0.94	0.67
0.86	1.50	0.93	1.50
0.80	2.67	0.89	2.67
0.71	4.16	0.86	4.16
0.65	6.00	0.83	6.00
0.57	8.16	0.80	8.16
0.49	13.49	0.72	13.49
0.44	20.15	0.66	20.15
0.43	28.15	0.59	28.15
0.42	37.48	0.55	37.48
0.41	48.14	0.51	48.14

Table 3: **Drainage relative permeability for two samples with high and moderate permeabilities**

High permeable sample		*Moderate permeable sample*	
Water Saturation	**Relative Permeability**	**Water Saturation**	**Relative Permeability**
1.00	0.00	1.00	0.00
0.87	0.00	0.90	0.00
0.82	0.036	0.87	0.024
0.66	0.109	0.74	0.059
0.57	0.145	0.63	0.071
0.52	0.181	0.57	0.094
0.41	0.416	0.53	0.106
0.39	0.507	0.50	0.129
0.38	0.616	0.47	0.235

Table 4: Components composition in weight % near the wellbore

Component	*Initial composition*	*Composition at the end of injection*
H_2O	91.09	88.62
CO_2	0.00	0.70
NaCl	7.41	8.62
$CaCl_2$	1.50	1.88

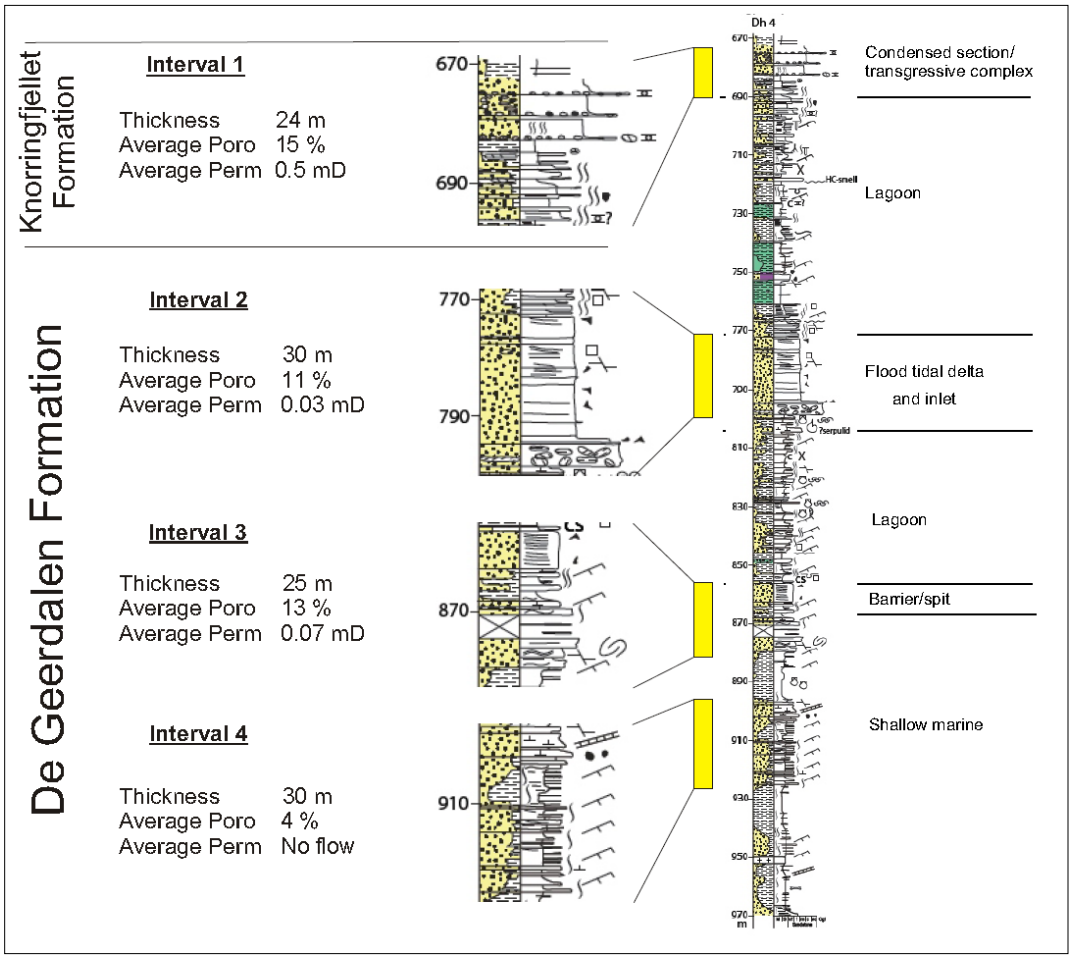

Figure 1: The potential intervals for injecting CO_2 storage (Tveranger, et al., 2009)

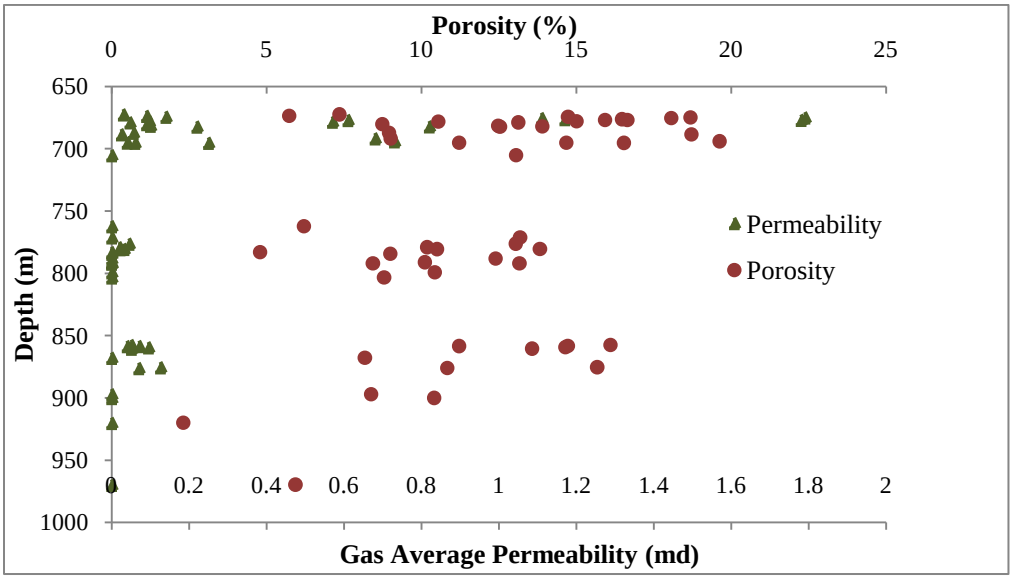

Figure 2: Porosity and permeability distribution

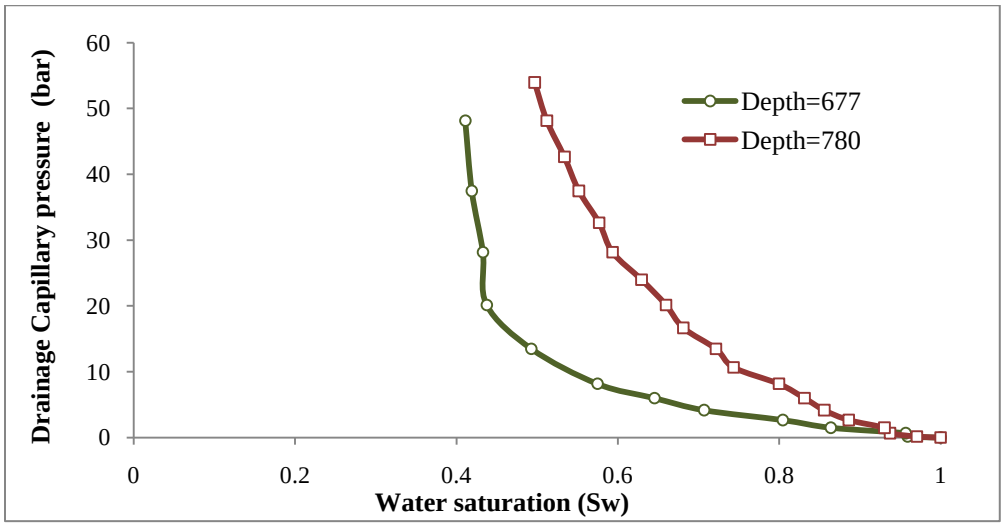

Figure 3: Drainage capillary pressure for air-water system

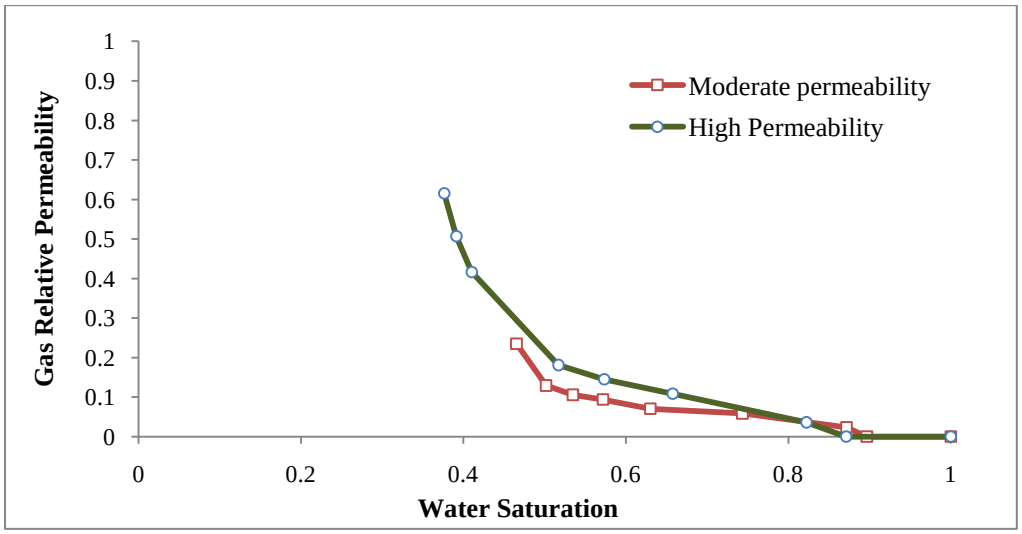

Figure 4: Drainage air relative permeability curve

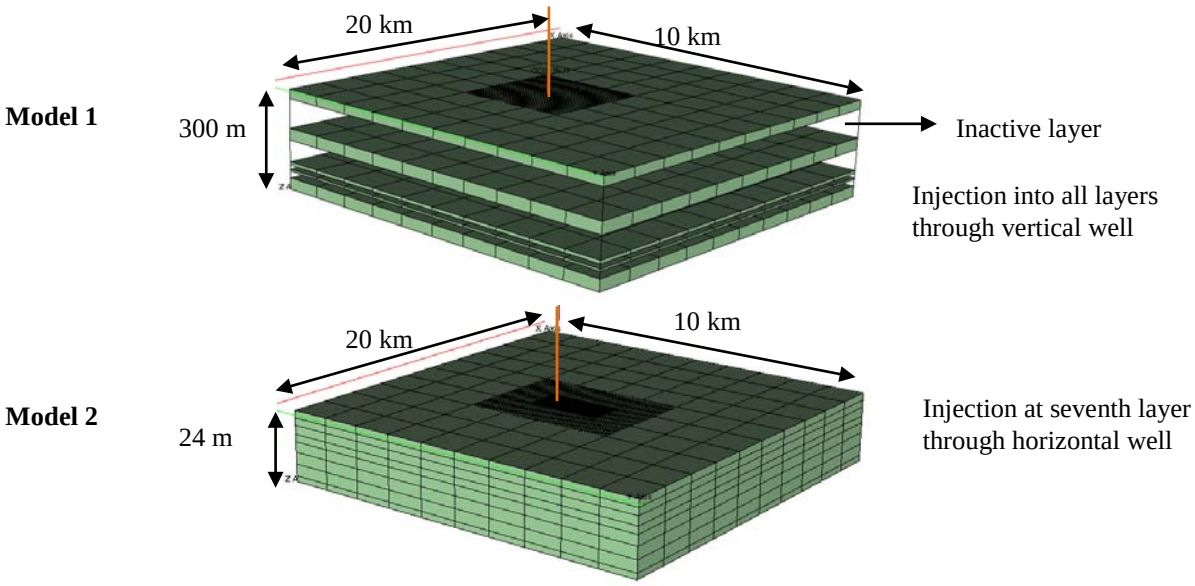

Figure 5: Model 1 and 2 geometries for simulation

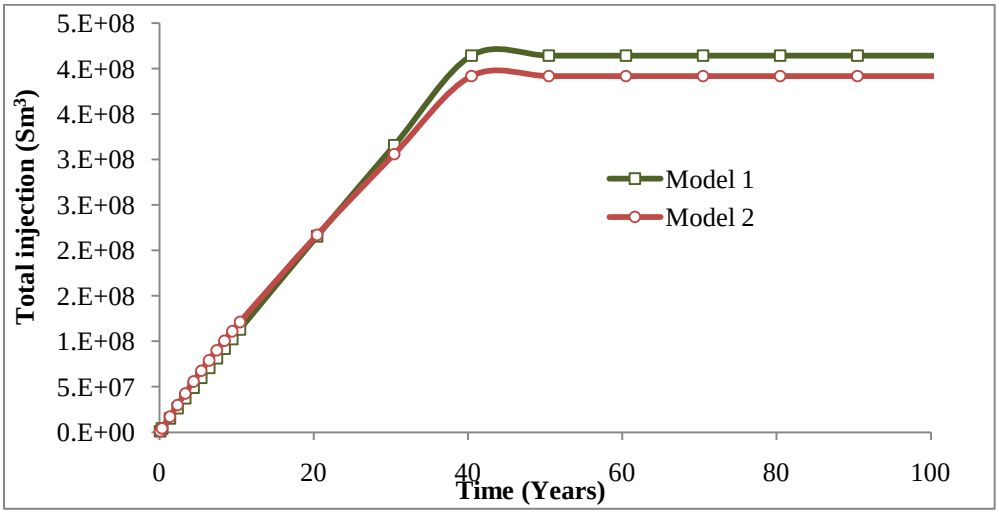

Figure 6: Comparing injectivity in model 1 and 2

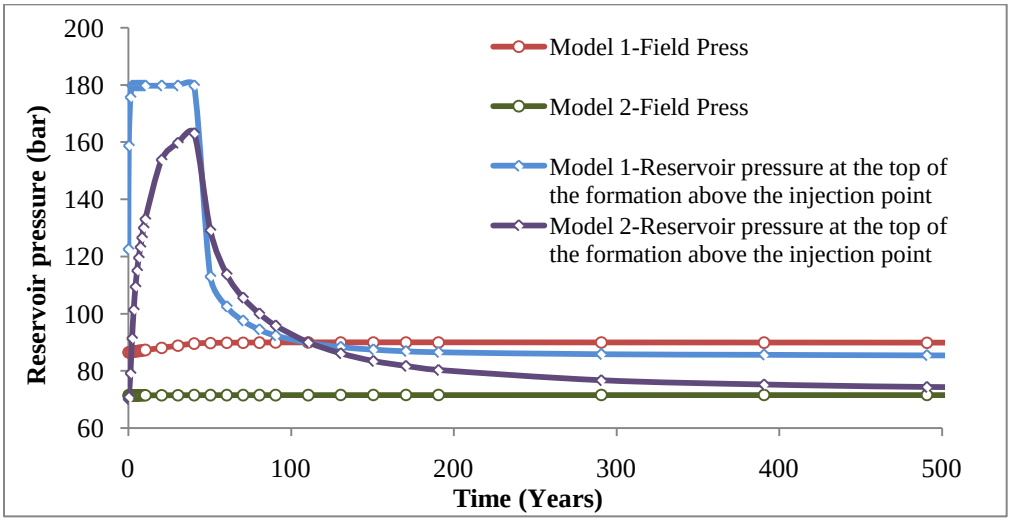

Figure 7: Comparing reservoir pressure in model 1 and 2

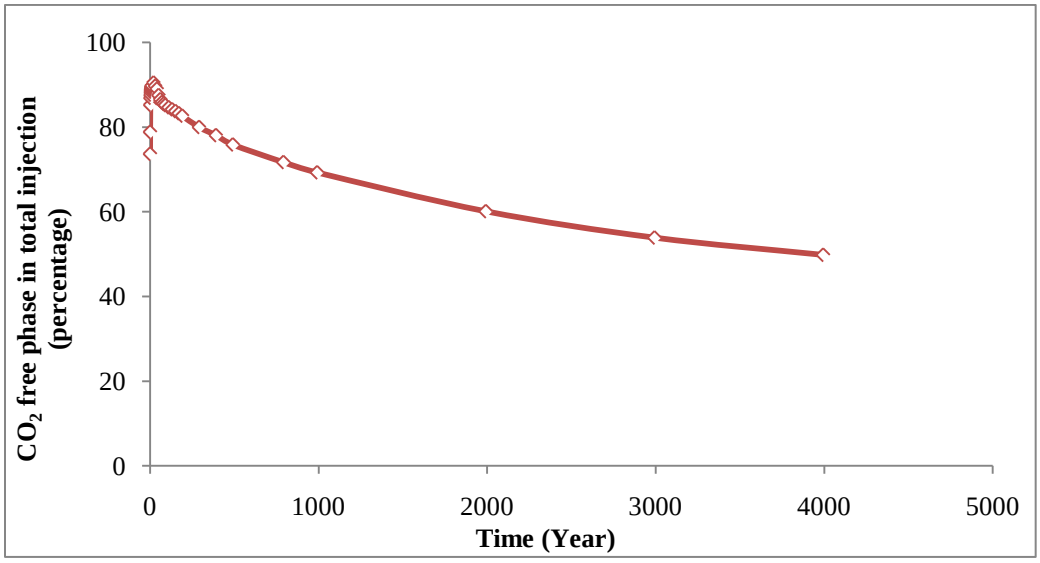

Figure 8: The percentage of CO_2 free phase in total injected CO_2

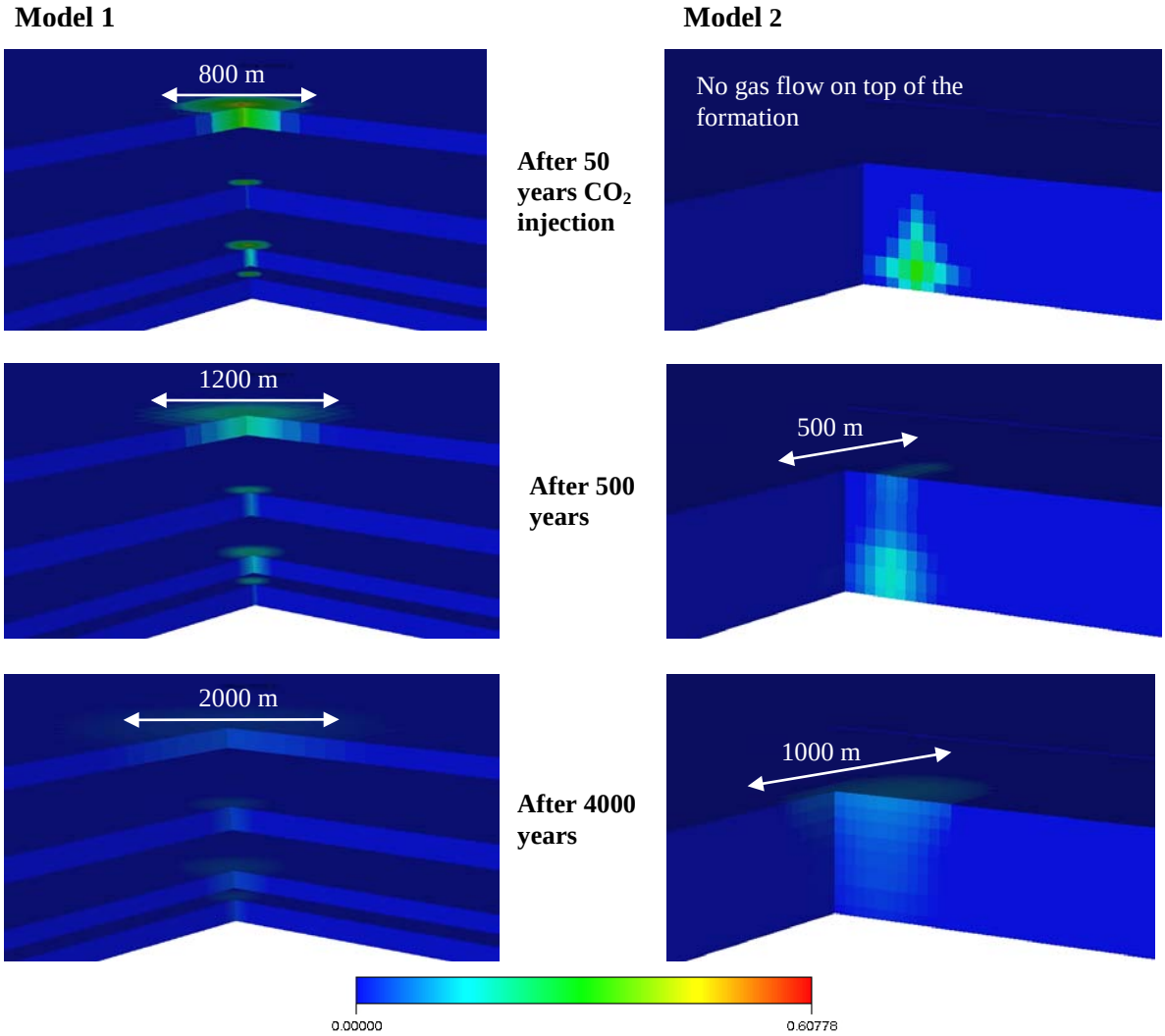

Figure 9: Pie section of CO_2 saturation and plume extent around the injection well at different time steps